Mapping afforestation and deforestation from 1974 to 2012 using Landsat time-series stacks in Yulin District, a key region of the Three-North Shelter region, China

Liangyun Liu · Huan Tang · Peter Caccetta · Eric A. Lehmann · Yong Hu · Xiaoliang Wu

Abstract The Three-North Shelter Forest Program is the largest afforestation reconstruction project in the world. Remote sensing is a crucial tool to map land use and land cover change, but it is still challenging to accurately quantify the change in forest extent from time-series satellite images. In this paper, 30 Landsat MSS/TM/ETM+ epochs from 1974 to 2012 were collected, and the high-quality ground surface reflectance (GSR) time-series images were processed by integrating the 6S atmosphere transfer model and a relative reflectance normalization algorithm. Subsequently, we developed a vegetation change tracking method to reconstruct the forest change history (afforestation and deforestation) from the time-series Landsat GSR images based on the integrated forest z-score (IFZ) model by Huang et al. (2009a), which was improved by multi-phenological IFZ models and the smoothing processing of IFZ data for afforestation mapping. The mapping result showed a large increase in the extent of forest, from 380,394 ha (14.8 % of total district area) in 1974 to 1,128,380 ha (43.9 %) in 2010. Finally, the land cover and forest change map was validated with an overall accuracy of 89.1 % and a kappa coefficient of 0.858. The forest change time was also successfully retrieved, with 22.2 % and 86.5 % of the change pixels attributed to the correct epoch and within three epochs, respectively. The results confirmed a great achievement of the ecological revegetation projects in Yulin district over the last 40 years and also illustrated the potential of the time-series of Landsat images for detecting forest changes and estimating tree age for the artificial forest in a semi-arid zone strongly influenced by human activities.

Keywords Remote sensing · Three-North Shelter Forest Program · Forest change · Time-series · Afforestation · Deforestation

L. Liu (✉) · H. Tang · Y. Hu
Key Laboratory of Digital Earth Science,
Institute of Remote Sensing and Digital Earth,
Chinese Academy of Sciences,
Beijing 100094, China
e-mail: liuliangyun@sina.com

P. Caccetta · E. A. Lehmann · X. Wu
Commonwealth Scientific and Industrial Research
Organisation (CSIRO), Division of Mathematics,
Informatics and Statistics (CMIS),
Private Bag 5,
Wembley, WA 6913, Australia

Introduction

Land-use and land-cover change is an important factor which affects the terrestrial carbon cycle and biodiversity (Chapin Iii et al. 2000; Foley et al. 2005; Vitousek et al. 1997). Forest biomass and productivity accounts for nearly 80 % of the total carbon estimated to be in the terrestrial above-ground biosphere (Waring and Running 2007). Human-induced forest changes, such as afforestation and deforestation, represent major sinks and sources of CO_2 and the associated greenhouse gas

fluxes (Hirsch et al. 2004; Law et al. 2004). Knowledge of the afforestation and deforestation history is necessary to understand atmospheric carbon budget (Schimel et al. 1997; Thornton et al. 2002).

The collection of Landsat images provides a unique data source for reconstructing forest change history at regional or global scale. National Aeronautics and Space Administration and the United States Geological Survey (USGS) developed a Landsat Data Distribution Policy for the distribution of global terrain-corrected data (L1T), making over 2.2 million images freely available via the Internet (Woodcock et al. 2008). Huang et al. (2009b) described a streamlined approach for producing imagery-ready-to-use (IRU) quality Landsat time-series stacks (LTSS). This approach consists of an image selection protocol, high-level preprocessing algorithms, and IRU quality verification procedures. Over the past 40 years, Landsat images have been widely used in forest change analysis (Goward and Williams 1997). Brandt et al. (2012) mapped the forest change in southwest China in response to the national logging ban and ecotourism using multi-date Landsat images (four epochs). Their analysis showed that logging rates decreased considerably from 1974 to 2009 and that forest cover increased from 62 % in 1990 to 64 % in 2009. Time-series analysis to determine forest change are preferred (Townshend et al. 2012), as applications based on two-dates or multi-dates of Landsat images may be strongly affected by phenology differences and bidirectional reflectance distribution function effects (Liu et al. 2009; Zhu et al. 2012). The availability of dense time series of Landsat images provides a chance to reconstruct forest disturbance and change history with higher temporal resolution (such as 1 year) and higher precision. For example, Caccetta et al. (2013) and Lehmann et al. (2013) used time-series Landsat imagery from 1972–2013 to identify changes in forest extent and trend respectively for the Australian continent at multiple epochs for the purpose of estimating forest changes associated with carbon accounting.

A vegetation change tracking algorithm was presented by Li et al. (2009a) and Huang et al. (2009a, b) to detect forest changes from a time-series of Landsat images. Li et al. (2009a) analyzed the wall-to-wall forest change patterns in Mississippi during the time period 1987–2005 from 132 Landsat TM and ETM+ scenes using a vegetation change tracker (VCT) algorithm and revealed a gradually decelerating forest fragmentation during the time period 1987–1993 and an accelerating

fragmentation during the period 1994–2005. Other application of VCT included that in Alabama, USA (Li et al. 2009a); Mississippi (Li et al. 2009b); eastern United States (Huang et al. 2009a); and the locations where LTSS have been assembled through the North American Forest Dynamics project (Goward et al. 2008; Huang et al. 2010). Huang et al. (2009a) used the VCT method for mapping forest disturbance with an overall accuracy of about 80 %. Most of these works were focused on mapping the disturbance (deforestation, fire, regrowth) over contiguous areas of high-density forest, and the application of the time-series of Landsat images for forest change mapping, especially afforestation in the semi-arid and sparsely forested regions, is still to be verified.

In 1978, the Chinese government initiated a significant ecological restoration project in North China, named The Three-North Shelter Forest Program (TNSFP), also known as the Great Green Wall. TNSFP is a huge ecological restoration effort being implemented in northwestern, northern, and northeastern China (english.forestry.gov.cn) and is also the largest ecosystem restoration project in the world. The program's aims were to increase the forest coverage in North China to effectively control sand storms and soil erosion, and also to improve ecological conditions and ecosystem services (Wu et al. 2009). According to the project's goal, it aimed to increase the forest area in the program regions by 35,083 million ha and increase the forest coverage from 5.05 % in 1977 to 14.95 % in 2050 (State Forestry Administration, P.R. China 2008). Numerous ecological restoration projects have been carried out in the TNSFP region, which has been suffering from serious sand storm and soil erosion. From 1978 to 2009, the forest coverage of the project area was raised from 5.05 % to 10.51 % (english.forestry.gov.cn). It is very important to examine the achievements of these ecological restoration projects by remote sensing. However, many TNSFP-related papers were focused on monitoring vegetation coverage in the TNSFP region using low-resolution remote sensing data, such as MODIS and AVHRR (Wu et al. 2009; Duan et al. 2011; Wang et al. 2011) or mapping forest changes using multi-temporal Landsat images based on visual interpretation or supervised classification (Yan et al. 2011; Pang et al. 2012).

The aims of the present study are: (1) to develop a method for afforestation and deforestation mapping

from the time-series Landsat TM/ETM+ images; (2) to examine the spatial and temporal accuracy of the afforestation and deforestation mapping in a semi-arid zone with strong human activities; and (3) to evaluate the afforestation effects of the ecological projects in key TNSFP regions.

## Study area and data acquisition

Study area

The TNSFP region covers 551 county-level administrative regions in 13 provinces in north China, with an extent of 4,480 km from east to west and ranging from 560 to 1,440 km from south to north. Its total area is 4,069 million km^2, accounting for 42.4 % of the total land area of China (Zha et al. 2007). The land cover types and range of the TNSFP region is illustrated in Fig. 1.

Yulin district is an important part of the TNSFP region, ranging from 107° 28′ E to 111° 15′ E, and from 36° 57′ N to 39° 34′ N. It consists of 12 counties (namely Yuyang, Shenmu, Fugu, Hengshan, Jingbian, Mizhi, Jia county, Dingbian, Suide, Wubao, Qingjian, and Zizhou) and covers an area of 43,578 km^2, accounting for 21.17 % of the total area of Shaanxi province (Zha et al. 2007). The elevation in Yulin district ranges from 585 to 1,907 m above mean sea level. In the north and west parts, it was covered by vegetated or bared desert, accounting for 42 % of the total area, while a loess hilly and gully region lies in the south and east parts, accounting for 58 % of its total area. The region's landforms gradually change from Mu Us Desert to north Shaanxi loess plateau. It exhibits a temperate semi-arid continental monsoon climate with the characteristics of being dry and windy in spring, hot during summer with most of rainfall, while dry and cold during winter. The mean annual temperature is about 10 °C, and the mean annual precipitation is about 400 mm, with most of the rainfall occurring in July and August (Williams et al. 2006).

Yulin district is an ecologically fragile region in the TNSFP region. The land cover types include vegetated dunes, mobile dunes, desert, cropland, and forest, as illustrated in Fig. 1. According to the survey data by the Yulin Forestry Administration, the afforestation area over the whole region reached 1.339 million acres (30.7 %) before 2010 (http://www.ylxww.com/show.aspx?id=17589&cid=42). The planted tree species include Chinese pine (*Pinus tabulaeformis*), poplar (*Populus alba*), *Sabina vulgaris* (*Savin juniper*), Scots pine (*Pinus sylvestris*), pagoda tree (*Styphnolobium japonicum*), and elm (*Ulmus rubra*).

Figure 2 shows examples of Landsat images in different years, wherein this display re-vegetation appears as dark-brown in color. The image sequence illustrates that most mobile dunes or desert were successfully vegetated in the last 30 years and that the mobile dune stripes, marked A, B, C, D, E, F in
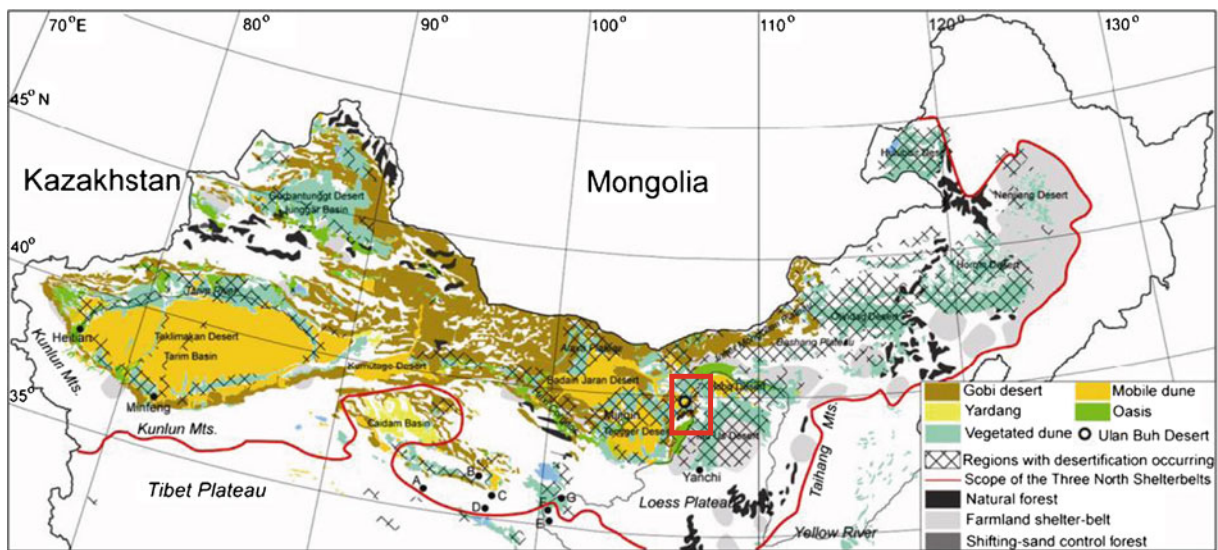
Fig. 1 The Three-North Shelterbelt Region and the study area (*central red rectangle*) (revised from Wang et al. 2010)

Fig. 2 Landsat images of the study area (RGB 742): a TM image (paths/rows 127–33 and 34) on 30 June 2009; b TM image (paths/rows 127–33 and 34) on 2 August 1986; c subset of TM images for location F shown in (a) and (b) (from *left to right*: 17 July 2010, 31 May 2001, and 2 August 1986), with dark-brown pixels corresponding to afforestation areas

(a)

(b)

(c)
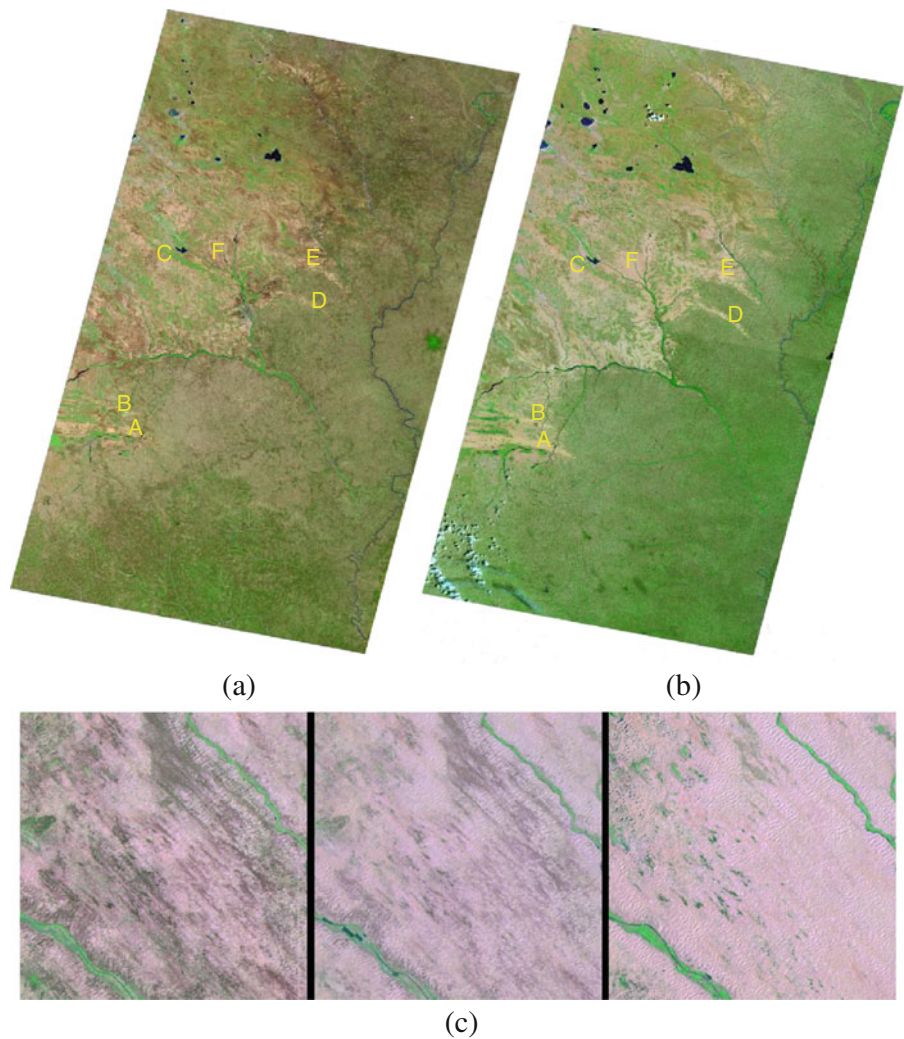
(Fig. 2a), were successfully fixed and vegetated. It is evident that the outcomes of the ecological revegetation projects in Yulin district were consistent with their goals.

Collection of Landsat temporal images

The Yulin district covers six Landsat TM/ETM+ images (paths 126, 127, and 128/rows 33 and 34). In order to avoid differences in acquisition date between paths, two Landsat scenes from path 127 were chosen as the study region. These scenes provide complete cover for seven counties of the Yulin district, including Shenmu, Yuyang, Jia county, Hengshan, Mizhi, Zizhou, and Qingjian counties, having a combined area of 25,682 km^2.

In this study, we collected 25 epochs of Landsat TM/ETM+ satellite images from 1986 to 2011 and another five epochs of Landsat MSS images from 1974 to 1978, as described in Table 1. The study area is covered by two Landsat TM scenes, namely path/row 127/33 and 127/34. The footprint of the Landsat MSS images is different from that of Landsat TM/ETM+, and we required two Landsat MSS paths (136 and 137) to cover the study area. Path 137 covers about 80 % of the study area, and another 20 % was filled in with path 136. All 30 epochs (70 scenes in total) were acquired with a quality higher than seven (minimal or no cloud contamination) during the vegetation growing season. Almost all forest species in this region are deciduous. Therefore, only images during growing season were selected to

Table 1 Acquisition dates (yyyy-mm-dd) of collected Landsat images (path 127 for TM/ETM+ sensor, paths 136 and 137 for MSS sensor)

Path/row	Acquisition date
127/33 and 34	2012-06-30, 2011-07-22, 2010-07-17, 2009-06-30, 2008-09-15, 2007-08-12, 2007-05-24, 2006-09-10, 2005-07-29, 2004-09-12, 2003-08-17, 2002-08-06, 2001-05-31, 2000-05-20, 1998-07-02, 1996-06-10, 1995-06-08, 1994-08-24, 1993-06-18, 1992-07-17, 1990-08-29, 1989-09-11, 1988-09-24, 1987-05-17, 1986-08-02
137/33 and 34	1978-08-01, 1977-08-15, 1976-09-25, 1975-04-22, 1974-05-24
136/33 and 34	1978-09-23, 1977-07-07, 1976-06-26, 1975-06-14, 1973-11-24

discriminate forest from non-vegetation covers and also to determine the deforestation or afforestation time.

The images were collected from the USGS Landsat archive (http://glovis.usgs.gov) and the China remote sensing satellite ground station (www.ceode.cas.cn). There were two epochs collected in 2007, and the image acquired on 24 May 2007 was employed to build the multi-phenological IFZ (integrated forest z-score) model (introduced later), and another image acquired on 12 August 2007 was selected to reconstruct the annual change of forest cover.

Image processing of Landsat time-series data

All Landsat images were sourced from either the USGS (via the download facility) or the China Remote Sensing Ground Station (RSGS). Standard level-one terrain-corrected (L1T) product, which were geometrically corrected orthorectified products by the data provider using standard systematic correction methods (Li et al. 2009b), were selected from the USGS site. Fast-formatted products without geometric correction and orthorectification were provided by the China RSGS.

All Landsat images were processed using the following steps to produce the time-series of ground reflectance data.

1. Orthorectification to a common spatial reference for the Landsat TM images from the China remote sensing satellite ground station, using an earth orbital model and ASTER 30 m DEM (digital elevation model) data from USGS and processed with a software developed by CSIRO (Caccetta et al. 2007). The Landsat TM image acquired on 30 June 2009 from USGS in L1T format was selected as the base image for geometric correction, orthorectification, and also normalization process of ground surface reflectance for other images. All

the orthorectified Landsat MSS, TM and ETM+ images were re-sampled to a 30 m resolution by linear interpolation.

2. Terrain illumination correction. All the Landsat images were corrected using a C-correction method (Teillet et al. 1982) and ASTER DEM (30 m) data, using software developed by CSIRO (Wu et al. 2004).

3. Image atmospheric correction for the base image. The base image (acquired on 3 June 2009) was first radiometrically corrected according to the calibration coefficients and methods described in Chander et al. (2009). Then, the top-of-atmosphere radiance image was corrected using an atmospheric correction algorithm adapted from the MODIS 6S radiative transfer approach (Vermote et al. 2002); the atmospheric parameters for the 6S model were taken from the MODIS atmospheric products, including MOD04 (L2 Aerosol), MOD05 (L2 total precipitable water vapor), and MOD07 (L2 temperature and water vapor profiles). We developed software to automatically complete this step, requiring as inputs only the filename of the Landsat image, the MODIS atmospheric products and DEM data.

4. Production of GSR images based on a relative normalization method. For such a long time-series of Landsat images, it is almost impossible to obtain the measured atmospheric parameters for atmospheric correction. Therefore, we developed a procedure to derive GSR products based on the relative radiance normalization algorithm (Cohen et al. 2003). An iterative re-weighted multivariate alteration detection algorithm by Cohen et al. (2003) was used to detect the invariant target pixels. The Landsat DN images from Step 2 were then matched to the GSR base image from Step 3 by least-square fitting for these invariant pixels, and the time-series Landsat GSR images were produced.

Figure 3 illustrates three GSR subset images produced with the above steps (location A marked in (Fig. 2a and b). All three ground reflectance images are displayed with the same histogram stretch parameters; the same colors can be observed across epochs for the same targets. This figure also illustrates the significant increase in forest cover, especially with large areas of afforestation after 2000. The mean reflectance spectra of the water pixels (area A1 in Fig. 3) and desert pixels (area A2 in Fig. 3) are summarized in Table 2. This result shows that the relative normalization method of Step 4 is satisfactory in producing high-precision time-series GSR images, with a GSR absolute error lower than 0.015 for all six reflectance bands of the three epochs.

Field data

In situ surveys were conducted from 20 to 22 October 2011 and 24 to 28 from May 2012. Fifteen sites were investigated for forest change mapping, distributed in four counties of the Yulin district, namely Jia county, Shenmu, Yuyang, Hengshan, Mizhi, Zizhou, and Qingjian. The variables recorded were forest type, tree density, tree diameter at breast height, and afforestation time. The afforestation time or land cover change time was investigated in situ by local forestry staff or determined using a tree-ring method or tree-node number method (only valid for pine trees). Photographs of the surrounding landscape were taken and localized by a handheld GPS. Finally, the 15 ground truth patches for afforestation mapping were located on the 22 July 2011 Landsat TM image according to the in situ GPS records. Figure 4 shows some typical in situ photos of afforestation sites in the Yulin district.

Methods

Multi-phenological forest z-score for forest mapping

Huang et al. (2009a) presented a vegetation change tracking model to automatically map the forest change history from time-series of Landsat images, which has proved to be able to detect most forest disturbance events including harvest, fire, and urban development (Huang et al. 2009a, 2010). An integrated forest z-score was designed to discriminate forest and non-forest pixels in multi-spectral images (Huang et al. 2009a).

With training forest pixels determined according to ground surveys or visual interpretation, the mean ($\overline{bi}$) and standard deviation (SD_i) of band i for the training forest samples can be calculated from the GSR image. The forest z-score (FZ_i) value for that band is defined as follows (Huang et al. 2009a):

$$FZi = \frac{\left(bi - \overline{bi}\right)}{SDi} \tag{1}$$

For multi-spectral images, the IFZ (integrated forest z-score) value of each pixel is then defined as (Shumway 1987; Huang et al. 2009a):

$$IFZ = \sqrt{\frac{1}{NB}\sum_{i=1}^{NB}(FZi)^2} \tag{2}$$

where NB is the number of bands used. For Landsat TM/ETM+ images, bands 3, 5, and 7 were used to calculate the IFZ values of each pixel (Huang et al. 2009a). For Landsat MSS images, bands 1, 2, and 4 were used to calculate the IFZ value (band 3 was excluded due to its high correlation with band 4).
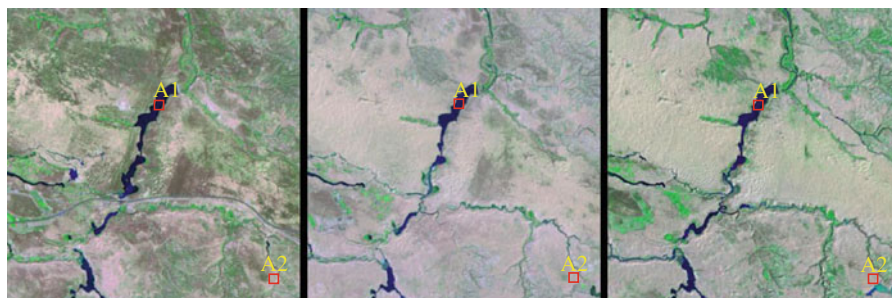

Fig. 3 Ground surface reflectance (GSR) images (RGB 742). From *left to right*: 17 July 2010, 31 May 2001, and 2 August 1986

Table 2 Landsat GSR spectra of the invariant targets in different epochs

	Water			Desert		
	1986	2001	2010	1986	2001	2010
B1	0.035	0.041	0.036	0.085	0.100	0.087
B2	0.069	0.075	0.061	0.178	0.190	0.180
B3	0.049	0.052	0.043	0.234	0.244	0.235
B4	0.034	0.039	0.032	0.326	0.331	0.339
B5	0.037	0.039	0.035	0.409	0.417	0.412
B7	0.035	0.037	0.033	0.406	0.417	0.412

Weather limitations (such as cloudy and fog) due to the monsoon climate mean that it is almost impossible to collect time series of Landsat images during the forest growth peak season (July and August). As shown in Table 1, the Landsat time-series images cover all the forest growth stages from May to September. Therefore, the phenological differences in IFZ scores should be considered, and it is almost impossible to retrieve the planting year from such IFZ curves fluctuating as a result of phenological differences, especially for sparse forest in the semi-arid loess region, such as the Yulin district. The spectral signature of known forest pixels within each image was used to normalize the images acquired at different time and growth season (Huang et al. 2009a). However, it is quite difficult to find the stable forest pixels in recent 40 years in Yulin district, and the forest growth and disturbance during such a long period cannot be neglected. Therefore, the multi-phenological IFZ models were built using the recent epochs (2007–2011) to normalize the phenological difference.
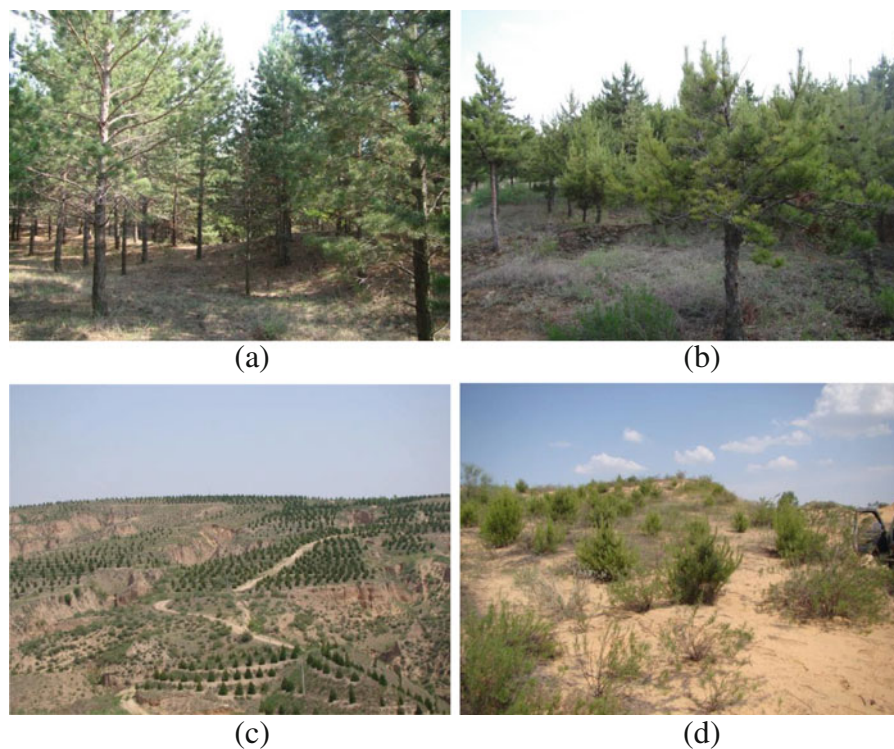
Fig. 4 Photos of different afforestation sites in the Yulin district: **a** afforestation of Scots pine in 1980; **b** afforestation of Chinese pine in 1980; **c** afforestation of *S. vulgaris* in 2003; **d** afforestation of Chinese pine in 2004

A set of persisting forest training sites (1,275 pixels) were selected according to in situ investigation and visual interpretation, to calculate statistical values as required in Eqs. 1 and 2, according to ground surveys and visual interpretation. IFZ models in different months (May to September) were built using five epochs from 2007 to 2011 and are summarized in Table 3. The growth difference between 2007 and 2001 was neglected for the stable forest training dataset, which was fixed across the five epochs. Therefore, we can calculate the IFZ data for the Landsat GSR images listed in Table 1 according the IFZ model given by Eq. 2 and the relative statistical parameters in Table 3, which reduces the phenological difference greatly. Finally, the time-series of IFZ images are calculated according to this procedure. The Landsat TM image acquired on 24 May 2007 was only used to build the IFZ model in late spring (May). It was not employed as one of the time-series GSR images to map forest changes because there was already another Landsat TM image in the growth peak season in 2007.

Based on these results, the impact that phenological differences would have on the IFZ curves can be easily evaluated. For instance, if the 22 July 2011 IFZ model was selected, the IFZ value of the reference forest spectrum of 15 September 2008 would be 0.728, which would effectively lead to a 0.728 phenological fluctuation in the IFZ curve between July and September (neglecting potential reflectance normalization errors).

For time-series of IFZ images, the cloud-contaminated (invalid) pixels were identified by their IFZ value (IFZ value greater than 6). These and other invalid pixels in Landsat ETM+SLC products (two epochs only) were replaced by the IFZ values of the nearest epoch.

Although the phenological impact was considered here, there were still small fluctuations for stable forest due to various causes such as inter-annual climate differences, image radiance normalization, spatial atmospheric differences, growth stage differences (less than half a month), etc. The increase of afforestation trees is typically gradual and smooth. Therefore, it is necessary to smooth the temporal IFZ curves to derive the exact planting year for the afforestation pixels. Savitzky and Golay (1964) proposed a simplified least-squares-fit convolution for smoothing a noise curve. In this study, the Savitzky–Golay filter was defined as a quadratic polynomial fitting function with a window size of 11, which proved to be efficient in smoothing the IFZ curves (Fig. 5). The relatively smaller variance in the IFZ values of the five Landsat MSS images (1974 to1978) also illustrated that the IFZ model based on Landsat MSS B1, B2, and B4 was not so sensitive to vegetation cover, compared with the IFZ values of the other Landsat TM/ETM+ images based on Landsat TM B3, B5, and B7.

Forest change mapping rules using the IFZ time-series data

As defined in Eqs. 1 and 2, the IFZ parameter has an inverse relationship with the likelihood of a pixel belonging to the forest class. If a pixel's reflectance

Table 3 Mean ($\overline{bi}$) and standard deviation (SD_i) values for forest z-score models in different months (May to September)

		B1	B2	B3	B4	B5	B7
2007-05-24	Mean	0.050	0.094	0.105	0.215	0.233	0.198
	SD	0.012	0.016	0.022	0.024	0.029	0.032
2010-06-17	Mean	0.028	0.065	0.082	0.206	0.218	0.172
	SD	0.014	0.024	0.032	0.032	0.045	0.051
2011-07-22	Mean	0.026	0.062	0.086	0.235	0.237	0.182
	SD	0.023	0.042	0.046	0.029	0.057	0.070
2007-08-12	Mean	0.057	0.101	0.108	0.251	0.254	0.204
	SD	0.007	0.014	0.020	0.031	0.037	0.039
2008-09-15	Mean	0.049	0.097	0.115	0.237	0.277	0.236
	SD	0.012	0.021	0.030	0.032	0.049	0.052
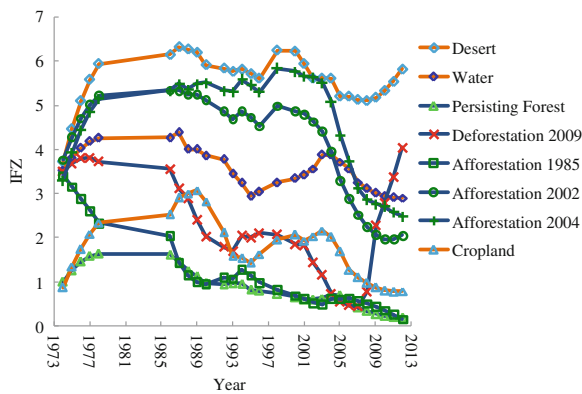
Fig. 5 Temporal IFZ curves for different land use and land cover change cases

spectrum is close to that of the forest training pixels (as listed in Table 3), its IFZ value will be close to 0 and this pixel would be labeled as forest. On the other hand, those pixels with high IFZ are more likely non-forest (as illustrated in Fig. 5).

IFZ thresholds for the identification of forest pixels and planting year

Assuming that the IFZ values of forest pixels exhibit a normal Gaussian distribution, the probability of a pixel being a forest pixel can be directly related to its IFZ scores using a Standardized Normal Distribution Table (Huang et al. 2010). In our study, over 98 % of the IFZ values of the investigated in situ (stable) forest pixels were less than 2.0; 99 % of the pixels had IFZ values less than 2.5, and 90 % less than 1.2. Therefore, a pixel is labeled as stable forest if its IFZ value is 1.2 or less and labeled as forest if its IFZ value is between 1.2 and 2.0, while an IFZ threshold of 2.5 is used to identify the planting year and non-vegetated pixels.

However, for some afforestation cases in bare desert areas (as illustrated, for instance, in Fig. 2c and the photo in Fig. 4d), the sandy background presents high reflectance, and the IFZ value was far higher than for bare soil or cropland. As a result, these afforestation pixels in the desert could not be detected with the above threshold values (2.0 for forest pixels and 2.5 to identify planting years). Most of these plantings occurred after 2000 under strong political requirements and economical funding supported by China's central government. For such cases, a monotonous decrease of IFZ (the smoothed IFZ data) with an amplitude greater than 2.0 and with a minimum IFZ

value lower than 2.5 (see "Afforestation 2004" curve in Fig. 5) was also used to identify a pixel as afforestation pixel. And the threshold for determining planting year was set as a value of 1.0 greater than the minimum IFZ in the recent 10 years.

For persisting forest, the IFZ value would remain very small over the study period. Accounting for disturbances such as cloud, haze if a pixel's IFZ values were all less than 2.0 except for three epochs, then it is identified as persisting forest.

Considering the gradual increase of afforestation plantings, the smoothed IFZ time-series data obtained by Savitzky–Golay filtering were used for afforestation mapping according to the above rules.

IFZ thresholds for the identification of deforestation

Deforestation typically causes a rapid increase of IFZ value. If the IFZ value increases by 1.5 or more from a low value less than 1.2 (stable forest) and maintains a high value greater than 2.5 after the increase, this pixel is identified as deforestation, and the year of initial increase is recorded as the felling year. The original IFZ time-series data were used to map deforestation.

Cropland mapping rules using IFZ time-series data

Parts of the Yulin district are heavily influenced by human activities, and there are numerous cropland regions surrounded by desert and forest. Where crops were planted and had significant canopy cover, the spectra of the pixels in these areas were similar to other natural vegetation such as forest and shrubs, making it challenging to discriminate the cropland for these periods. However, the time-series of Landsat images provides a chance to discriminate cropland according to the phenological variations for different crops over time.

As illustrated in Table 1, the acquisition time of the Landsat images ranges from May to September, which covers almost the entire growth season for crops in Yulin district. The crops include winter wheat, spring maize, rice, millet, and potato. In different growth stages, the reflectance spectra would vary greatly, even for one crop. Consequently, cropland regions would typically exhibit rapid fluctuations under different growth stages or different crops in the temporal IFZ curves. In this study, more than five fluctuations with amplitude greater than 1.0 in the original IFZ time-

series, with a minimum value lower than 1.2, are taken as an indication of a pixel being cropland.

Non-vegetation cover mapping rules using IFZ and GSR reflectance time-series data

For non-vegetated covers, such as water and bare land, the IFZ value typically remains high during the study period. Accounting for the inter-annual changes of water cover and cloud contamination, if a pixel's IFZ values are greater than 2.5 except for less than four epochs, it is labeled as non-vegetated pixel. Subsequently, water pixels are discriminated from bare land. The spectral reflectance of water is very low in the near-infrared (NIR) and short-wave infrared bands (almost zero for clear water), but the NIR reflectance of bare land is high (almost always greater than 30 %). Considering the water turbidity in rivers (especially the Yellow River), the presence of water is deemed likely if the band 7 reflectance of the Landsat TM/ETM+ image is less than 10 %. Thus, if this case occurs five times or more in all 25 epochs (MSS images were not used here due to their low resolution), a pixel is finally labeled as water, while otherwise retaining its bare land classification.

Land cover and forest change mapping algorithm

According to the above classification rules, we built an algorithm to map the different land covers and forest changes (afforestation and deforestation), as shown in Fig. 6. The mapping rules for the identification of forest changes and cropland are described above. C1 and C2 in Fig. 6 are the afforestation and deforestation cases associated with the afforestation and deforestation mapping rules, respectively. The corresponding planting and felling years were also retrieved in this step according to the methods described above.

Results and validation

Afforestation and deforestation mapping from 1974 to 2012 in Yulin District

The Landsat images listed in Table 1 were all processed according to our image processing steps, leading to the production of the time-series Landsat GSR images. The time-series IFZ images were also calculated according to the IFZ models for different growth season (listed in
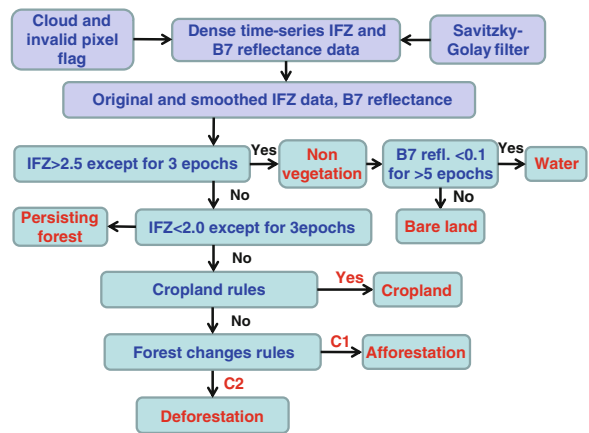

Fig. 6 Flowchart to map land covers and forest changes using the time-series of IFZ and reflectance data

Table 2). For the Landsat MSS data, the IFZ images of path 136 and 137 were calculated independently (the IFZ model was different for different growth seasons), and image mosaicing was applied to the two paths' IFZ images. Finally, the time-series of IFZ images and reflectance data (band 7 only) was used as input to the mapping algorithm described in Fig. 6, leading to the production of land cover and forest change information, including the planting and felling years for the forest changes pixels. All land covers were mapped into 56 classes, including water, persisting forest, bare land, cropland, 26 afforestation classes from 1975 to 2010, and 26 deforestation classes from 1975 to 2012.

Figure 7 shows the land cover and forest change mapping results over Yulin district from 1974 to 2012, which highlights the great achievements of the local afforestation projects in the past 40 years. In Fig. 8, the amounts of afforestation and deforestation between 1974 and 2012 are summarized according to the political extents of the Yulin district (only seven counties) and Jia county. It clearly shows a big forest increase in Yulin district (seven counties) from 1974 to 2012, with 2001 being the most significant growth year with a total afforestation area of 209,369 ha. Another afforestation peak occurred around 1977. These two afforestation peaks agree with the start of TNSFP in 1977 and another strong political promotion of afforestation after 2000, through an initiative proposed by Premier Zhu Rongji in 1999 called "Returning cultivated land to forest and mountain greening." There was also a small peak of deforestation (2,984 ha) in 2009, clearly visible in the plots in Fig. 8, which was caused by basic
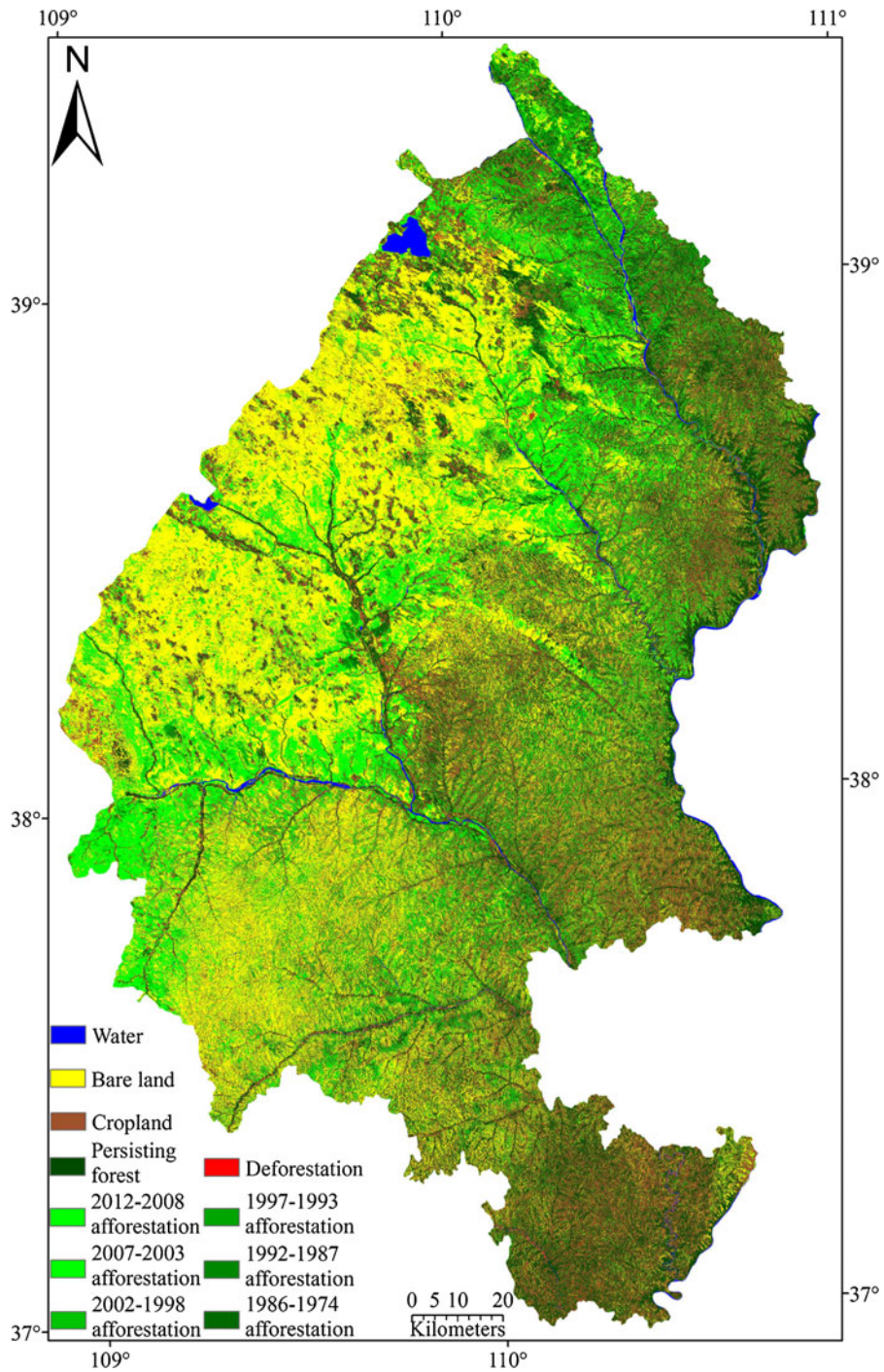
Fig. 7 Land cover and forest change mapping from 1974 to 2012 over Yulin district

infrastructure construction projects (such as construction, city and airport development, mining industry, etc.) promoted by the government after the global economic crisis in 2008.

The forest cover areas and forest changes are also summarized in Table 4 for the Yulin district (only seven counties) and Jia county (political borders). The persisting forest cover area is 375,796 ha (14.6 %) and
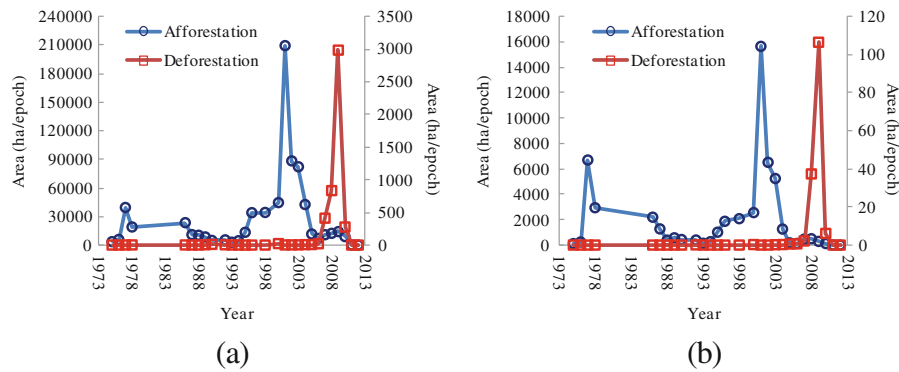
Fig. 8 Epoch-wise afforestation (*blue lines, left-hand vertical axis*) and deforestation (*red lines, right-hand vertical axis*) increments between 1974 and 2012: **a** Yulin district (seven counties), **b** Jia county

44,983 ha (22.1 %) for Yulin district and Jia county, respectively, which was directly mapped according to the persisting forest IFZ rule as described in the "Methods" section. The results show a big increase in forest area over the last 40 years in Yulin district. The afforestation and deforestation inventory data were not available for public or scientific research, and it is difficult to link the remotely sensed afforestation data with the government's inventory afforestation data. The ground survey and biomass harvest experiment was supported by the Forest Bureau of Jia county, who also provided information of the forest extends of Jia county in 1975 and 2010. According to this forest inventory data, the forested land area of Jia county increased from 59,747 ha in 1975 to 115,380 ha in 2010, corresponding to a percentage of the forested land increasing from 28 % (1975) to 56 % (2010). According to the remote sensing results shown in Table 4, the forest cover of Jia county increased from 45,251 ha (22.2 %) in 1974 to 98,483 ha (48.5 %) in 2010. Due to the definition of forest cover in this paper being quite different from the definition of forested land in the inventory data, the afforestation area from remote sensing mapping is about 7 % lower than that of the inventory area. However, the results presented in this work remain basically consistent with the inventory data provided by the Forest Bureau of Jia county, with a similar percentage-wise increase of total forested area (about 26 %) over the 35-year period. Furthermore, the forest cover of Yulin district (seven counties) increased from 380,394 ha (14.8 %) in 1974 to 1,128,380 ha (43.9 %), which is also consistent with the survey data by the Yulin Forestry Administration with an afforestation area of 30.6 % over the whole Yulin District (12 counties)

before 2010 (http://www.ylxww.com/show.aspx?id=17589&cid=42).

Validation of the land cover and forest change mapping

Validation of land cover products mapped from satellite images is typically based on independent in situ ground truth data or visual interpretation. In this paper, the land use and land cover change mapping was validated using the in situ investigation sites. Seventeen patches were selected as ground truth data according to in situ investigations and also the 2011 Landsat TM image. The validation results of the land cover and forest change mapping is listed in Table 5. The result showed that forest cover and forest change time were successfully mapped from the temporal IFZ data, and cropland was also discriminated with a producer's accuracy of 84.7 % and a user's accuracy of 81.4 %.

All the land covers and forest changes in Table 5 were merged into six classes, namely water, bare land, cropland, persisting forest, afforestation, and deforestation. The confusion matrix for this six class mapping was calculated and is shown in Table 6. These results show that the land covers were successfully classified with an overall accuracy of 89.1 % and a Kappa coefficient of 0.858. The producer's and user's accuracy for afforestation was 78.4 % and 87.9 %, respectively. The producer's and user's accuracy for deforestation was 89.1 % and 100 %, respectively.

The planting and felling years were also retrieved from the time-series Landsat GSR images, leading to the 26 afforestation classes and 26 deforestation classes. The temporal detection accuracy of forest changes was also calculated according to Table 5, with the

Table 4 Forest area (hectares) and coverage in Yulin district (seven counties) and Jia county from 1974 to 2010

Year	Yulin district				Jia county			
	Afforestation	Deforestation	Forest	Coverage	Afforestation	Deforestation	Forest	Coverage
2010	8,899	277	1,128,380	43.9 %	118	6	98,483	48.5 %
2009	14,133	2984	1,119,758	43.6 %	288	106	98,370	48.4 %
2008	12,316	834	1,108,609	43.2 %	497	37	98,188	48.3 %
2007	10,851	412	1097127	42.7 %	463	2	97,729	48.1 %
2006	6,908	20	1,086,688	42.3 %	127	1	97,268	47.9 %
2005	11,591	8	1,079,800	42.0 %	173	1	97,142	47.8 %
2004	42,565	6	1,068,216	41.6 %	1,260	0	96,969	47.7 %
2003	82,201	3	1,025,658	39.9 %	5,240	0	95,710	47.1 %
2002	88,349	2	943,460	36.7 %	6,513	0	90,470	44.5 %
2001	209,371	2	855,113	33.3 %	15,647	0	83,957	41.3 %
2000	44,576	22	645,744	25.1 %	2,557	0	68,311	33.6 %
1998	34,240	0	601,190	23.4 %	2,077	0	65,754	32.4 %
1996	34,020	0	566,950	22.1 %	1,872	0	63,677	31.3 %
1995	13,417	0	532,930	20.8 %	1,014	0	61,806	30.4 %
1994	4,567	0	519,513	20.2 %	264	0	60,791	29.9 %
1993	3,004	1	514,946	20.1 %	144	0	60,527	29.8 %
1992	5,459	4	511,943	19.9 %	397	0	60,383	29.7 %
1990	4,901	11	506,488	19.7 %	437	0	59,986	29.5 %
1989	8,523	5	501,598	19.5 %	571	0	59,549	29.3 %
1988	10,284	0	493,080	19.2 %	387	0	58,978	29.0 %
1987	10,951	1	482,796	18.8 %	1,272	0	58,591	28.8 %
1986	23,529	2	471,845	18.4 %	2,193	0	57,319	28.2 %
1978	18,991	2	448,318	17.5 %	2,939	0	55,126	27.1 %
1977	39,470	2	429,329	16.7 %	6,697	0	52,187	25.7 %
1976	5,884	0	389,861	15.2 %	240	0	45,491	22.4 %
1975	3,583	0	383,977	15.0 %	114	0	45,251	22.3 %
1974	0	0	380,394	14.8 %	0	0	45,137	22.2 %
Persisting forest			375,796	14.6 %			44,983	22.1 %

results provided in Table 7. The forest change time was quite good, with 22.2 % of pixels exactly retrieved, and 86.5 % of the pixels having a discrepancy of less than three epochs. This result illustrates the potential of the time-series of Landsat images for the detection of tree age in artificial forests, even in a semi-arid zone.

Conclusion

Landsat time-series images provide a historical record of land use and land cover change. In this paper, we developed a method to map the forest changes (afforestation and deforestation) in a semi-arid zone with strong human activities based on the time-series GSR Landsat images and the IFZ model presented by Huang et al. (2009a). The land covers and forest changes from 1974 to 2012 were successfully reconstructed from the time series of GSR Landsat images (29 epochs) in Yulin district, Shaanxi province, China, which is a key part of the TNSFP region. The land cover and forest change maps were validated using 17 ground-truth patches, with an overall accuracy of 89.1 % and a kappa coefficient of 0.858. The forest change times were also successfully retrieved, with 22.2 % of change pixels exactly retrieved and 86.5 % correctly identified within less than three

Table 5 Validation results for the land cover and forest change mapping (pixel counts)

Class	Bare land	Crop land	Water	2004 S1	2003 S2	2003 S3	2002 S1	1985 S1	1982 S1	1980 S2	1981 S1	1980 S4	1980 S1	1975 S2	1965 S1	Persisting forest	D2009 S1	Total
Bare land	1,302			15	5	2	54												1,378
Cropland		500				48	10				1		5		4	15	31	614
Water			306															306
2010	9																	9
2009	16																	16
2008	4						2											6
2007	1						4											5
2006	2	1		1			9											13
2005				16			25											41
2004	3	8		5		4	115											135
2003		3		1	4	41	64											113
2002		1			1	46	26	1										75
2001						71	20	3	1	1								96
2000		3				3	1	1								1		9
1998						2	1											3
1996						1	1		1					1		4		8
1995							1	1								1		3
1994		7																7
1993		1																1
1992										1								1
1990		2							2	1								5
1989		6					1	5	1	4			1			4		22
1988		1					3	7	5	4	2	7				11		40
1987		1					2	7	1	5	2	8		1				27
1986		16					2	70	14	45	8	7	1	19		5		187
1978		3					1	37	5	30	11		8	16		2		113
1977		2						11	2	23	9		8	5		3		63
Persisting Forest		35				3		43	3	29	7		10	6	26	559	6	727
D2009																	116	116
Total	1,337	590	306	38	10	221	342	186	35	143	40	22	33	48	30	605	153	4,139

Classes 1977–2010 are the afforestation classes from 1977 to 2010, D2009 is the deforestation class in 2009. S1 to S4 correspond to the forest species Chinese pine, poplar, *S. vulgaris*, and *P. sylvestris*, respectively

Table 6 Confusion matrix for the six class land cover and forest change mapping

	Bare land	Cropland	Water	Afforestation	Persisting forest	Deforestation	Total
Bare land	1,302			76			1,378
Cropland		500		64	19	31	614
Water			306				306
Afforestation	35	55		877	31		998
Persisting forest		35		101	585	6	727
Deforestation						116	116
Total	1,337	590	306	1,118	635	153	4,139

Overall accuracy 89.1 %, Kappa coefficient=0.858

epochs, which also illustrates the potential of the time series of Landsat images for the detection of tree age in artificial forests, even in a semi-arid zone.

The forest change mapping from the time-series Landsat GSR images clearly shows a big forest increase in Yulin district (seven counties) from 380,394 ha (14.8 %) in 1974 to 1,128,380 ha (43.9 %) in 2010. The largest afforestation occurred in 2001 and another peak occurred around 1977. These two afforestation peaks agree with the start of TNSFP in 1978 and another strong political promotion and funding for afforestation in 1999. The small deforestation peak in 2009 is also corroborated by the basic infrastructure construction projects promoted by the government after the global economic crisis in 2008. These results confirm the great success achieved by the ecological projects in Yulin district over the last 40 years.

In reconstructing the history of forest changes in a semi-arid zone with strong human activities, the following observations were particularly important.

1. A high quality of image preprocessing was indispensable. In this paper, we developed a relative reflectance normalization method to build the time-series GSR image stacks, with a GSR normalization difference less than 0.015 for all six reflectance bands of three different epochs (17 July 2010, 31 May 2001, and 2 August 1986), which was the basis for the quantitative analysis of forest changes from time-series Landsat images. The terrain radiance correction supported by high-resolution DEM data was required for rugged area.

2. The spectral variance of sparse forests in a semi-arid zone was higher than for forests (Huang et al. 2009a, 2010; Li et al. 2009a, b), and it is more challenging to retrieve the planting time from Landsat images acquired during different growth seasons. In this paper, we presented a multi-phenological IFZ model (Table 3), which significantly eliminates this phenological influence.

3. Considering the gradual growth characteristics of afforestation, the IFZ time series was smoothed by a Savitzky–Golay filter (Savitzky and Golay 1964) to remove the fluctuations caused by various disturbances. The afforestation year was successfully retrieved from the smoothed IFZ time-series curve. The original (raw) IFZ data were still used to determine other cases such as deforestation, cropland, water, bare land, and persisting forest.

4. The phenological information provided by the time-series Landsat image acquired at different growth seasons was different for different land covers, although it was challenging to retrieve the exact afforestation time. The fluctuations in the time-series IFZ curves due to phenological differences in cropped areas were successfully used to discriminate cropland from persisting forest and other forest change cases.

One limitation, however, is that we could not discriminate shrubs from forest using the time-series Landsat GSR images. The presented afforestation and

Table 7 Temporal detection accuracy of forest changes (epoch difference)

	0	≤1	≤2	≤3	≤5
Percent	22.2 %	57.8 %	73.6 %	86.5 %	97.4 %

deforestation data thus included both forest and shrub regions, which was also regarded as afforestation by the Chinese forest department. Other remaining challenges include discriminating between different afforestation types and also between the different sparse vegetation types in a semi-arid zone with strong human activities.

References

Brandt, J. S., Kuemmerle, T., Li, H., Ren, G., Zhu, J., & Radeloff, V. C. (2012). Using Landsat imagery to map forest change in southwest China in response to the national logging ban and ecotourism development. *Remote Sensing of Environment, 121*, 358–369.

Caccetta, P., Furby, S., O'Connell, J., Wallace, J., & Wu, X. (2007). Continental monitoring: 34 years of land cover change using Landsat imagery. In, *32nd International Symposium on Remote Sensing of Environment* (pp. 25–29)

Caccetta, P.A., Furby, S., Wallace J., Wu, X., Richards, G. and Waterworth, R. (2013). Long-Term monitoring of the Australian land cover change using Landsat data: Development, implementation and operation, in Global Forest Monitoring from Earth Observation, Achard and Hansen (editors), Boca Raton, FL, CRC press. ISBN 978-1-4665-5201-2

Chander, G., Markham, B. L., & Helder, D. L. (2009). Summary of current radiometric calibration coefficients for Landsat MSS, TM, ETM+, and EO-1 ALI sensors. *Remote Sensing of Environment, 113*, 893–903.

Chapin Iii, F. S., Zavaleta, E. S., Eviner, V. T., Naylor, R. L., Vitousek, P. M., Reynolds, H. L., et al. (2000). Consequences of changing biodiversity. *Nature, 405*, 234–242.

Cohen, W. B., Maiersperger, T. K., Gower, S. T., & Turner, D. P. (2003). An improved strategy for regression of biophysical variables and Landsat ETM+ data. *Remote Sensing of Environment, 84*, 561–571.

Duan, H., Yan, C., Tsunekawa, A., Song, X., Li, S., & Xie, J. (2011). Assessing vegetation dynamics in the Three-North Shelter Forest region of China using AVHRR NDVI data. *Environmental Earth Sciences, 64*, 1011–1020.

Foley, J. A., DeFries, R., Asner, G. P., Barford, C., Bonan, G., Carpenter, S. R., et al. (2005). Global consequences of land use. *Science, 309*, 570–574.

Goward, S. N., & Williams, D. L. (1997). Landsat and earth systems science: Development of terrestrial monitoring. *Photogrammetric Engineering and Remote Sensing, 63*, 887–900.

Goward, S. N., Masek, J. G., Cohen, W., Moisen, G., Collatz, G. J., Healey, S., et al. (2008). Forest disturbance and North American carbon flux. *Eos, Transactions of the American Geophysical Union, 89*, 105–116.

Hirsch, A. I., Little, W. S., Houghton, R. A., Scott, N. A., & White, J. D. (2004). The net carbon flux due to deforestation and forest re-growth in the Brazilian Amazon: Analysis using a process-based model. *Global Change Biology, 10*, 908–924.

Huang, C., Goward, S. N., Schleeweis, K., Thomas, N., Masek, J. G., & Zhu, Z. (2009a). Dynamics of national forests assessed using the Landsat record: Case studies in eastern United States. *Remote Sensing of Environment, 113*, 1430–1442.

Huang, C., et al. (2009b). Development of time series stacks of Landsat images for reconstructing forest disturbance history. *International Journal of Digital Earth, 2*, 195–218.

Huang, C., et al. (2010). An automated approach for reconstructing recent forest disturbance history using dense Landsat time series stacks. *Remote Sensing of Environment, 114*, 183–198.

Law, B. E., Turner, D., Campbell, J., Sun, O. J., Van Tuyl, S., Ritts, W. D., et al. (2004). Disturbance and climate effects on carbon stocks and fluxes across Western Oregon USA. *Global Change Biology, 10*, 1429–1444.

Lehmann, E. A., Wallace, J. F., Caccetta, P. A., Furby, S. L., & Zdunic, K. (2013). Forest cover trends from time series Landsat data for the Australian continent. *International Journal of Applied Earth Observation and Geoinformation, 21*, 453–462.

Li, M., Huang, C., Zhu, Z., Shi, H., Lu, H., & Peng, S. (2009a). Assessing rates of forest change and fragmentation in Alabama, USA, using the vegetation change tracker model. *Forest Ecology and Management, 257*, 1480–1488.

Li, M., Huang, C., Zhu, Z., Wen, W., Xu, D., & Liu, A. (2009b). Use of remote sensing coupled with a vegetation change tracker model to assess rates of forest change and fragmentation in Mississippi, USA. *International Journal of Remote Sensing, 30*, 6559–6574.

Liu, L., Jing, X., Wang, J., & Zhao, C. (2009). Analysis of the changes of vegetation coverage of western Beijing mountainous areas using remote sensing and GIS. *Environmental Monitoring and Assessment, 153*, 339–349.

Pang, G., Dong, X., Song, X., Li, B., & Ma, R. (2012). Remote sensing monitoring of forest land change in Hexi corridor since construction of the Three-North Shelterbelt Project. *Journal of Desert Research, 32*, 037–042.

Savitzky, A., & Golay, M. J. E. (1964). Smoothing and differentiation of data by simplified least squares procedures. *Analytical Chemistry, 36*, 1627–1639.

Schimel, D. S., Participants, V., & Braswell, B. H. (1997). Continental scale variability in ecosystem processes: Models, data, and the role of disturbance. *Ecological Monographs, 67*, 251–271.

Shumway, R. H. (1987). Statistics and data analysis in geology. *Technometrics, 29*, 492–492.

State Forestry Administration, P. R. C. (2008). *30 years development report of the Three-North Shelter Forest system construction*. Beijing: China Forestry Publishing House.

Teillet, P., Guindon, B., & Goodenough, D. (1982). On the slope-aspect correction of multispectral scanner data. *Canadian Journal of Remote Sensing, 8*, 84–106.

Thornton, P. E., Law, B. E., Gholz, H. L., Clark, K. L., Falge, E., Ellsworth, D. S., et al. (2002). Modeling and measuring the effects of disturbance history and climate on carbon and water budgets in evergreen needleleaf forests. *Agricultural and Forest Meteorology, 113*, 185–222.

Townshend, J. R., Masek, J. G., Huang, C., Vermote, E. F., Gao, F., Channan, S., et al. (2012). Global characterization and monitoring of forest cover using Landsat data: Opportunities and challenges. *International Journal of Digital Earth, 5*, 373–397.

Vermote, E. F., El Saleous, N. Z., & Justice, C. O. (2002). Atmospheric correction of MODIS data in the visible to middle infrared: First results. *Remote Sensing of Environment, 83*, 97–111.

Vitousek, P. M., Mooney, H. A., Lubchenco, J., & Melillo, J. M. (1997). Human domination of earth's ecosystems. *Science, 277*, 494–499.

Wang, X. M., Zhang, C. X., Hasi, E., & Dong, Z. B. (2010). Has the Three North Forest Shelterbelt Program solved the desertification and dust storm problems in arid and semi-arid China? *Journal of Arid Environments, 74*, 13–22.

Wang, Q., Zhang, B., Dai, S., Zou, Y., Ma, Z., & Zhang, Y. (2011). Dynamic changes in vegetation coverage in the Three-North Shelter Forest Program based on GIMMS AVHRR NDVI. *Resources Science, 8*, 1613–1620.

Waring, R. H., & Running, S. W. (2007). *Forest ecosystems: Analysis at multiple scales*. San Diego: Academic Press.

Williams, D. L., Goward, S., & Arvidson, T. (2006). Landsat: Yesterday, today, and tomorrow. *Photogrammetric Engineering and Remote Sensing, 72*, 1171–1178.

Woodcock, C. E., Allen, R., Anderson, M., Belward, A., Bindschadler, R., Cohen, W., et al. (2008). Free access to Landsat imagery. *Science, 320*, 1011–1013.

Wu, X., Furby, S., & Wallace, J. (2004). An approach for terrain illumination correction. In, *The 12th Australasian Remote Sensing and Photogrammetry conference proceedings, Fremantle, Western Australia* (pp. 18–22)

Wu, Y., Zeng, Y., Wu, B., Li, X., & Wu, W. (2009). Retrieval and analysis of vegetation cover in the Three-North Regions of China based on MODIS data. *Chinese Journal of Ecology, 28*, 1717–1718.

Yan, Q., Zhu, J., Hu, Z., & Sun, O. (2011). Environmental impacts of the shelter forests in Horqin Sandy Land, northeast China. *Journal of Environmental Quality, 40*, 815–824.

Zha, Y., Liu, Y., & Deng, X. (2007). A landscape approach to quantifying land cover changes in Yulin, Northwest China. *Environmental Monitoring and Assessment, 138*, 139–147.

Zhu, Z., Woodcock, C. E., & Olofsson, P. (2012). Continuous monitoring of forest disturbance using all available Landsat imagery. *Remote Sensing of Environment, 122*, 75–91.